# Supporting Information

## Enhancing Polysulfide Conversion in Lithium-Sulfur Batteries through the Synergistic Effect of 2,6-Dihydroxyanthraquinone and Co Atoms

Huijuan You[a,1], Fangfang Liu[b], Hanxiao Wang[c], Zining Wang[d], Xuyun Wang[a,*], Boshen Zhang[a], Kuanshuo Tang[a], Jianwei Ren[e,*], Rongfang Wang[a,*]

[a] College of Chemical Engineering, Qingdao University of Science and Technology, Qingdao, 266042, China

[b] Shandong Peninsula Blue Economy and Engineering Research Institute, Shandong Engineering Laboratory for Clean Utilization of Chemical Resources, Weifang University of Science and Technology, Shouguang, Weifang, 262700, China

[c] Qingdao Institute of Bioenergy and Bioprocess Technology, Chinese Academy of Sciences, Shandong Energy Institute, Qingdao New Energy Shandong Laboratory, Qingdao 266101, China

[d] School of Chemical Science and Engineer, Tongji University, 1239 Siping Road, Shanghai 200092, China

[e] Department of Chemical Engineering, University of Pretoria, cnr Lynnwood Road and Roper Street, Hatfield 0028, South Africa

*Corresponding author.

E-mail address: wangxy@qust.edu.cn (X. Wang); jianwei.ren@up.ac.za (J. Ren); rfwang@qust.edu.cn (R. Wang)

Number of pages: 11

Number of Tables: 3

Number of Figures: 14

Number of References: 16

**Preparation of Co-C substrate:**

0.03 mmol of $Co(NO_3)_2 \cdot 6H_2O$ and 1 g of peptone were dissolved in 2 mL of deionized water. The mixture was sonicated for 5 to 10 min until completely dissolved. Next, the solution was placed in the refrigerator to freeze for 12 h and form an ice block. The frozen block was then transferred to a freeze dryer and lyophilized for 12 h. After drying, the resulting sample was mixed with 10 g of NaCl and ball-milled at 550 rpm for 3 h. Following ball milling, the mixture was heated to 900 °C in a tube furnace under a nitrogen atmosphere at a heating rate of 5 °C $min^{-1}$, maintaining this high temperature for 1 h. After cooling to room temperature, the carbonized product was washed and dried in an oven at 60 °C.

**Preparation of DHAQ/Co-C sample:**

60 mg of Co-C sample was dispersed in 20 mL of a 0.05 mM DHAQ solution. The mixture was magnetically stirred for 30 min. Then, the product was centrifuged, and the resulting solid was dried in a forced air oven at 60 °C for 6 h.

**Preparation of S@Co-C and S@DHAQ/Co-C samples:**

Co-C and DHAQ/Co-C were ground with sublimed sulfur in a mass ratio of 2:3 for 30 min. In an argon-filled glove box, the mixture was placed in a preheated oven at 155 °C and allowed to react for 12 h to obtain the S@Co-C and S@DHAQ/Co-C samples.

**Preparation of $Li_2S_6$ solutions:**

$Li_2S$ and sublimed sulfur in a molar ratio of 1:5 was added to a mixed solvent of 1,3-dioxolane and dimethoxyethane (DME/DOL, v/v = 1:1). The mixture was stirred at 60 °C for 24 h to obtain a 0.2 M $Li_2S_6$ solution. Additionally, a 5 mM $Li_2S_6$ solution was prepared using the same method.

**Adsorption Experiment**

5 mg of Co-C and DHAQ/Co-C samples were added separately to 5 mL of 5 mM $Li_2S_6$ solution. The mixtures were allowed to stand for 2 h to observe any color changes.

**Physical Characterization**

In situ synchrotron radiation tests were conducted using the Shanghai Synchrotron Radiation Facility BL08U1A beamline. X-ray diffraction (XRD) analysis was performed using the MiniFlex 600 instrument from Rigaku Corporation, with a scanning rate of 10° $min^{-1}$ over a 2θ range of 10−80°. A Carl Zeiss Ultra Plus scanning electron microscope (SEM) was employed for morphology analysis. Transmission electron microscopy was conducted using a JEOL JEM-2000FX instrument. A UV-5800 PC UV spectrophotometer was utilized to measure absorbance in the wavelength range of 200−400 nm.

**Electrochemical Performance Testing**

The S@DHAQ/Co-C composite, conductive carbon black (Super P), and the binder polyvinylidene fluoride (PVDF) were mixed in a mass ratio of 7:2:1 and dissolved in N-methyl-2-pyrrolidone (NMP) under stirring. The resulting slurry was then coated onto aluminum foil current collectors and dried in an oven at 60 °C for 12 h to form the sulfur electrode. Lithium metal (diameter: 15.6 mm, and thickness: 0.45 mm.) was used as the anode, with Celgard 2400 (diameter: 16 mm) serving as the separator. The electrolyte comprised 1.0 M lithium bis(trifluoromethanesulfonyl)imide (LiTFSI) in a 1:1 volume ratio of dimethoxyethane (DME) and 1,3-dioxolane (DOL), supplemented with 1.0% lithium nitrate ($LiNO_3$). The button cells were assembled in an argon-filled glove box using CR2032 stainless steel battery casings. Unless otherwise specified, the typical sulfur loading in the electrode (diameter: 12 mm) ranged from approximately 1.19 mg $cm^{-2}$, with an electrolyte-to-sulfur (E/S) ratio of about 20 μL $mg^{-1}$. Furthermore, thermogravimetric analysis revealed that the actual sulfur content of S@DHAQ/Co-C is 59.77%, and all specific capacity data in the manuscript are calculated based on the actual sulfur content.

For symmetric cells, DHAQ/Co-C, Super P, and PVDF are mixed in a mass ratio of 8:1:1 and dissolved in NMP solvent to form a slurry, which is then coated onto carbon paper and dried in a forced air oven at 60 °C. A 0.2 M $Li_2S_6$ solution (60 μL) is used as the electrolyte for the assembly of the symmetric cell. Constant current charge-discharge tests were conducted on a Neware battery system

with a voltage range of 1.7−2.8 V. Cyclic voltammetry (CV) and electrochemical impedance spectroscopy (EIS) measurements were performed using a CHI 650D electrochemical analyzer. The frequency range for the EIS tests was from 100 kHz to 10 mHz, and all electrochemical tests were carried out at room temperature.

For the CV measurements, the scanning rate was set at 0.1 mV $s^{-1}$, and the voltage range was 1.7−2.8 V. The fitted peak current at scanning speeds ranging from 0.1 to 0.5 mV $s^{-1}$ can be analyzed using the Randles-Sevcik equation:

$$I_P = (2.69 \times 10^5) \times n^{1.5} \times A \times D_{Li}^{0.5} \times C_{Li} \times v^{0.5}$$

where $I_P$ is the peak current (A), $n$ is the number of reaction electrons ($n$=2), $A$ is the electrode area, $D_{Li}$ is the $Li^+$ diffusion coefficient, $C_{Li}$ is the $Li^+$ concentration in the electrolyte, and $v$ is the potential scan rate.

**Theoretical Calculations**

The calculations were performed using the Gaussian 09 software with the density functional theory (DFT) method B3LYP at the 6-311G(D) basis set level, employing the empirical keywords related to Gaussian 09 (em=gd3bj). All structures were optimized and verified to ensure the absence of imaginary frequencies. The lowest unoccupied molecular orbital (LUMO) and the highest occupied molecular orbital (HOMO), along with the electrostatic surface potential (ESP), were plotted and visualized using Multiwfn and Visual Molecular Dynamics (VMD).

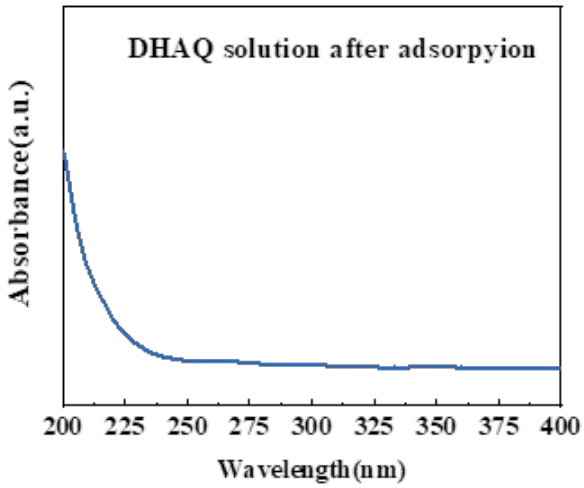

**Fig. S1.** UV-visible absorption spectrum of DHAQ solution after adsorption by carbon powder.

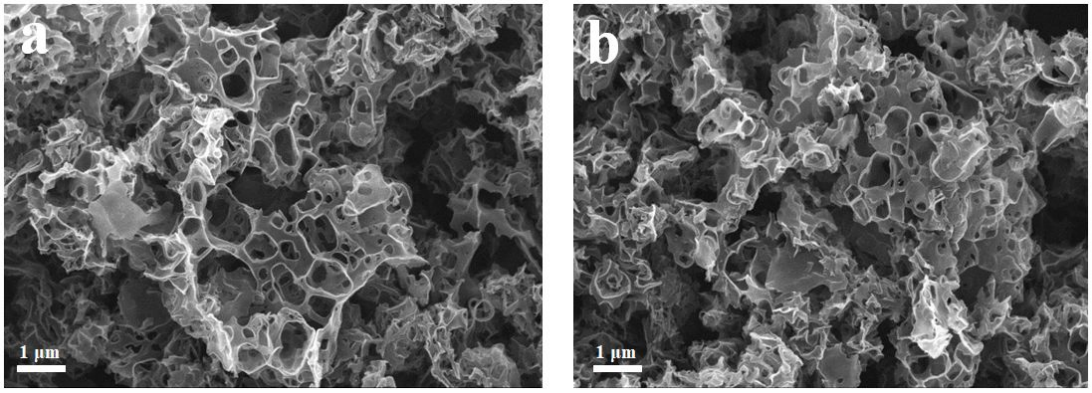


**Fig. S2.** SEM images of samples: (a) Co-N-C, (b) DHAQ/Co-N-C.

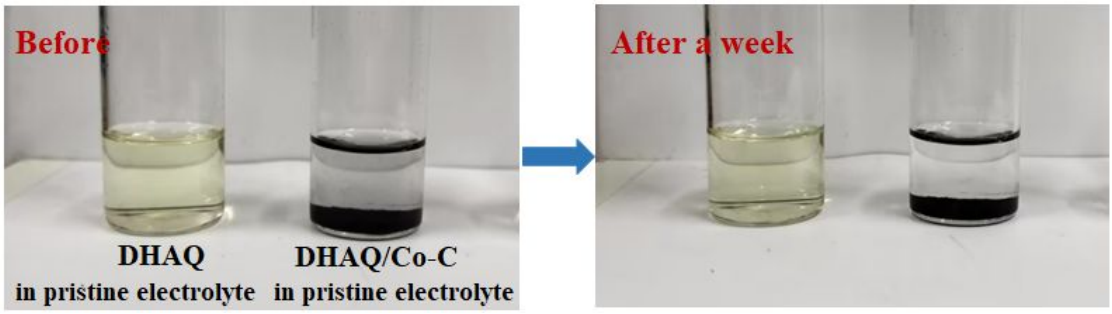


**Fig. S3.** Digital Photos of DHAQ and DHAQ/Co-C samples dispersed in pristine electrolyte (1.0 M LiTFSI in DOL/DME = 1:1 Vol% with 1.0% $LiNO_3$) before and after one week.

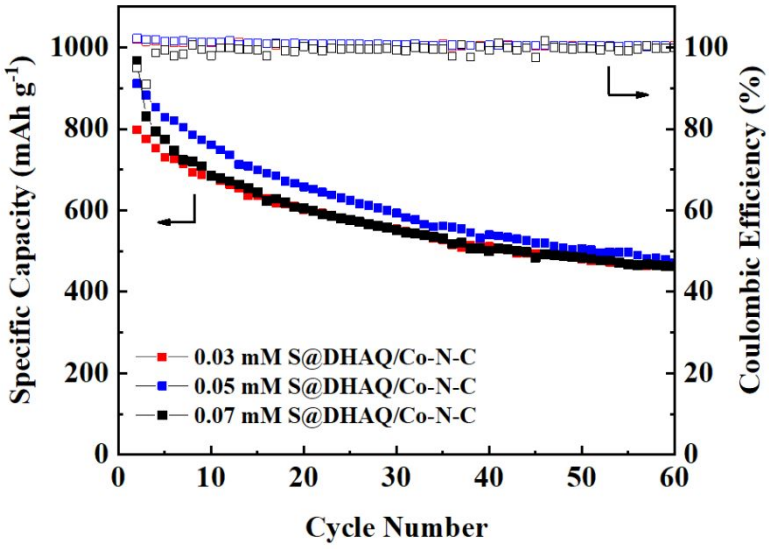


**Fig. S4.** Long cycling performance curves of the S@DHAQ/Co-C sample with various DHAQ loading contents, tested at a current rate of 0.2 C.

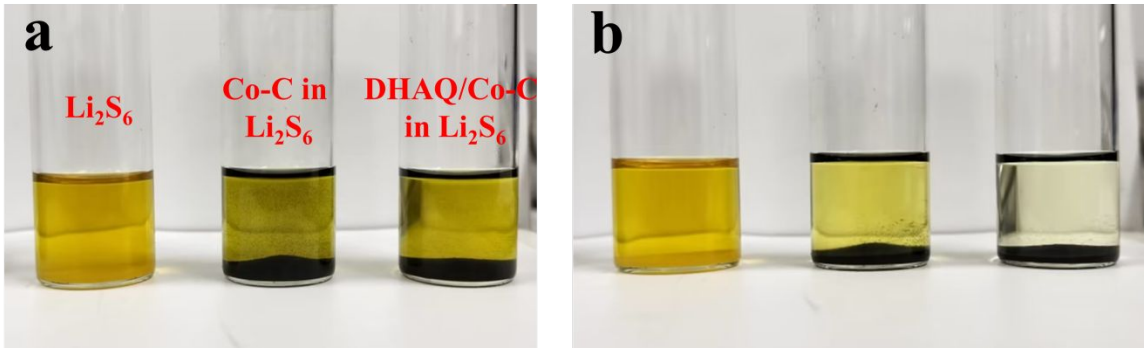


**Fig. S5.** Static adsorption test results of $Li_2S_6$ solution after adding Co-C and DHAQ/Co-C samples.

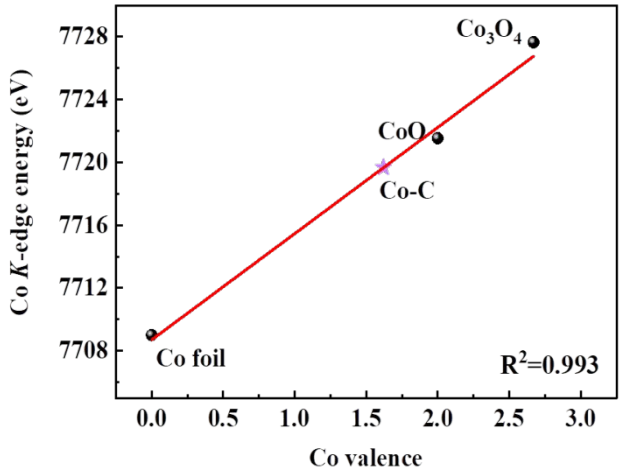


**Fig. S6.** K-space oscillation fitting of Co-C cathodes and reference materials derived from the correspond linear fitting curve ding Co K-edge XANES spectra.

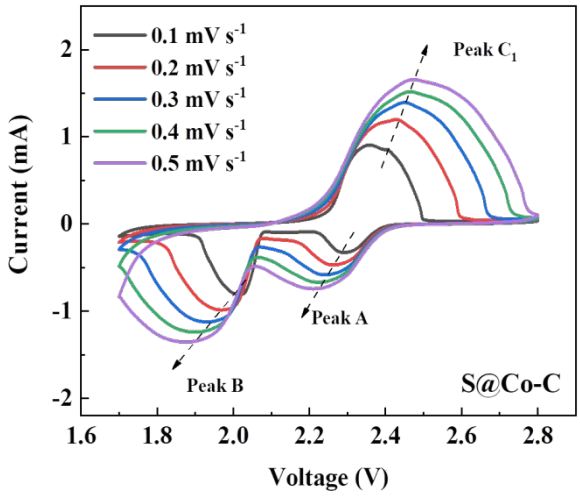


**Fig. S7.** CV curves of S@Co-C sample scanned at 0.1−0.5 mV $s^{-1}$.

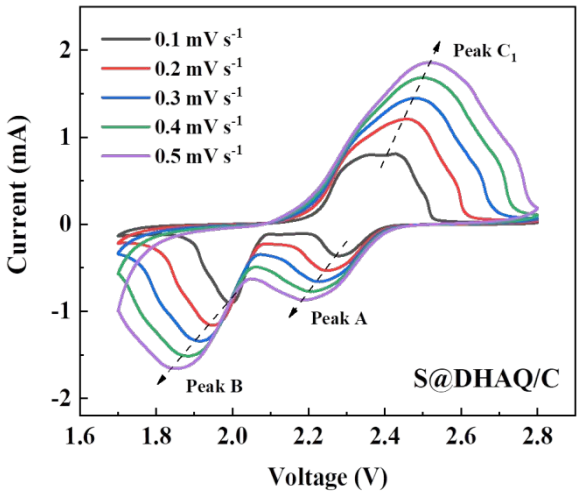


**Fig. S8.** CV curves of S@DHAQ/C sample scanned at 0.1−0.5 mV $s^{-1}$.

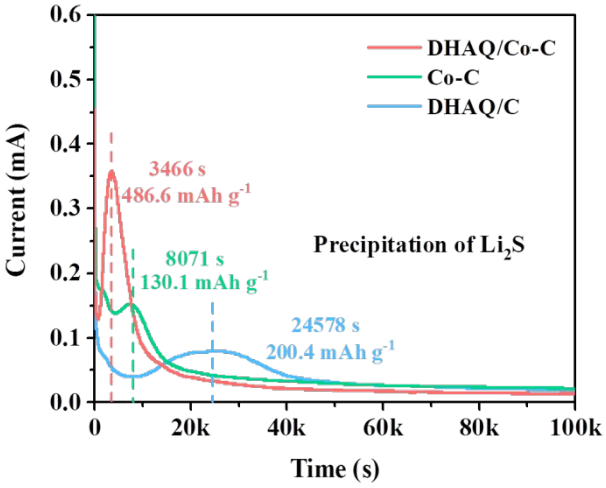


**Fig. S9.** Deposition curves of $Li_2S$ on the surfaces of DHAQ/C, Co-C, and DHAQ/Co-C electrodes at 2.05 V.

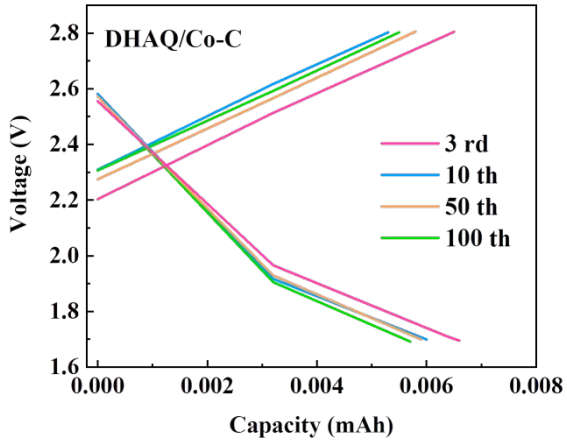


**Fig. S10.** Charge and discharge curves of the DHAQ/Co-C sulfur-free carbon cathode sample.

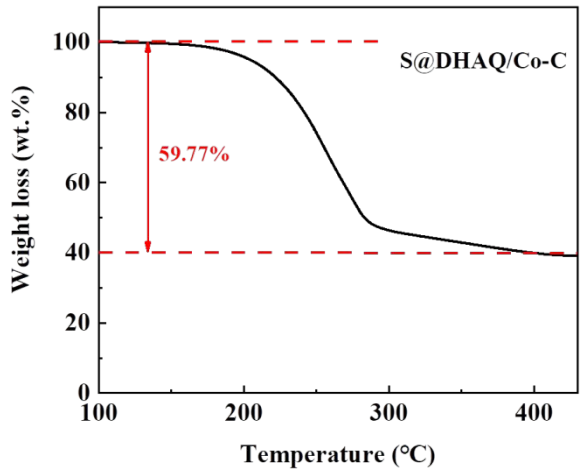


**Fig. S11.** Thermogravimetric (TGA) curve of S@DHAQ/Co-C sample.

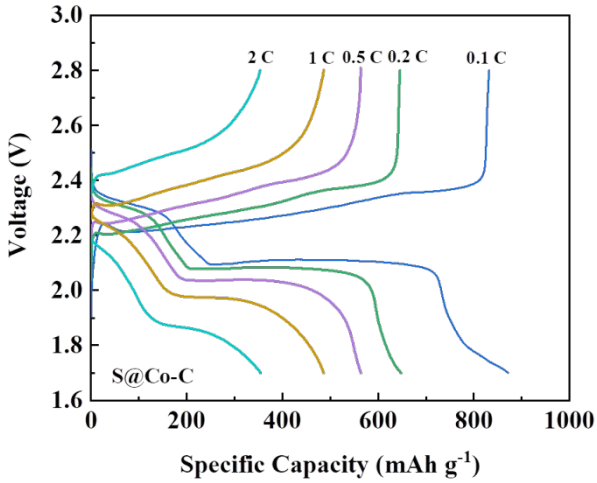


**Fig. S12.** Charge-discharge curves of S@Co-C sample at different current densities.

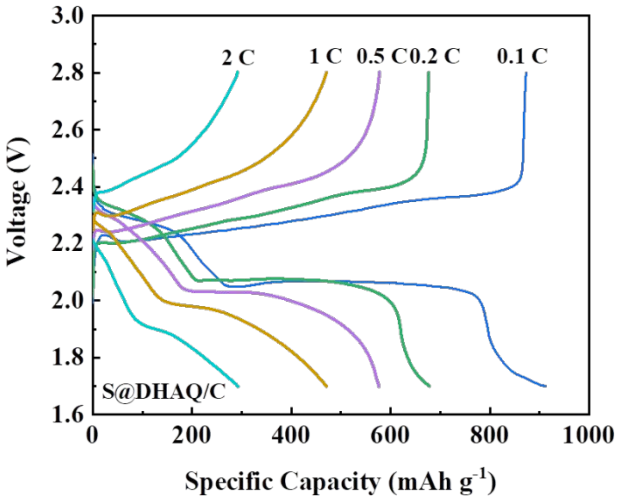


**Fig. S13.** Charge-discharge curves of S@DHAQ/C sample at different current densities.

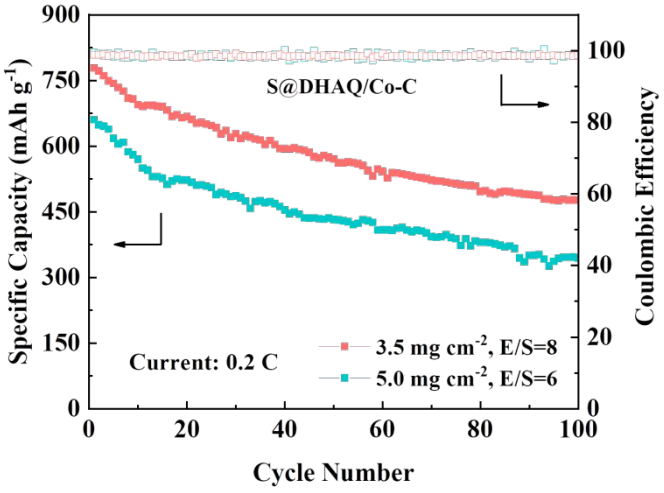


**Fig. S14.** Cycling stability of S@DHAQ/Co-C electrode at 0.2 C under sulfur loadings of 3.5 mg $cm^{-2}$ with E/S = 8 μL $mg^{-1}$ and 5.0 mg $cm^{-2}$ with E/S = 6 μL $mg^{-1}$.

**Table S1.** Structural parameters of the Co-N-C catalysts extracted from the EXAFS fitting.

| Sample | Scattering pair | Coordination number | Bond lengh R(Å) | R factor (100%) |
|---|---|---|---|---|
| Co-N-C | Co-N | 3.75 | 1.84 | 0.020 |

**Table S2.** $Li^+$ diffusion coefficients of the S@Co-N-C and S@DHAQ/Co-N-C samples.

| $D_{Li}^+$ ($cm^2$ $s^{-1}$) | A (cathodic peak) $S_8$→LiPS ($Li_2S_n$, 4≤n≤8) | B (cathodic peak) LiPS ($Li_2S_n$, 2≤n<4) →$Li_2S_2$/$Li_2S$ | $C_1$ (anodic peak) $Li_2S_2$/$Li_2S$→LiPS ($Li_2S_n$, 2≤n<4) | $C_2$ (anodic peak) LiPS ($Li_2S_n$, 4≤n≤8) → $S_8$ |
|---|---|---|---|---|
| S@DHAQ/C | $1.56*10^{-9}$ | $2.65*10^{-9}$ | $5.59*10^{-9}$ | -- |
| S@Co-C | $4.75*10^{-9}$ | $4.97*10^{-9}$ | $9.17*10^{-9}$ | -- |
| S@DHAQ/Co-C | $5.68*10^{-9}$ | $6.81*10^{-9}$ | $1.27*10^{-8}$ | $1.27*10^{-8}$ |

**Table S3.** Performance comparison with other electrodes reported in literature.

| Material type | Initial capacity (mAh $g^{-1}$) | High rate capacity (mAh $g^{-1}$) | Capacity decay rate per cycle | Ref. |
|---|---|---|---|---|
| PG-DAAQ | 1198/0.1 C | 899/1 C | 0.143%/1 C/200 | [1] |
| MB-AQ/rGO/S | 1291/0.1 C | 884/1 C | 0.005%/1 C/700 | [2] |
| Cu-$CeO_{2-x}$@CNF | 1188/0.5 C | 1058/2 C | 0.046%/2 C/800 | [3] |
| LLTO/S | 1180/0.1 C | 1050/0.2 C | 0.19%/0.2 C/100 | [4] |
| $Fe_3O_4$/FeP@C─S | 1402/0.1 C | 1093/1 C | 0.126%/1 C/300 | [5] |
| CoSA-N-C@S | 1574/0.05 C | 883/1 C | 0.035%/1 C/1000 | [6] |
| CoP@S | 1020/0.2 C | 1280/0.5 C | 0.059%/0.5 C/1000 | [7] |
| CC@CoSNC/$CoCp_2$−S | 1540/0.1 C | 904/0.5 C | 0.053%/0.5 C/300 | [8] |
| APC/S | 744/0.16 C | 1016/0.5 C | 0.035%/0.5 C/800 | [9] |
| TiN-NA | 1214/0.48 C | 960/0.96 C | 0.059%/0.48 C/500 | [10] |
| TiO@C-HS/S | 1190/0.2 C | 1066/0.5 C | 0.082%/0.5 C/500 | [11] |
| F-$TiO_2$ | 1260/0.24 C | 970/0.96 C | 0.097%/0.96 C/500 | [12] |
| S/NQ-rGO | 1254/0.1 C | 1204/1 C | 0.089%/1 C/500 | [13] |
| CNT@S | 1139/0.1 C | 794/0.5 C | 0.061%/0.1 C/200 | [14] |
| HEA-CNT/S | 948/0.3 C | 767/2 C | 0.054%/2 C/1000 | [15] |
| Co-VN@NC | 891/0.2 C | 644/1 C | 0.07%/1 C/500 | [16] |
| S@DHAQ/Co-C | 1385/0.1 C | 572/1 C | 0.062%/1 C/600 | This work |

# References


[1] Lai, T.; Manthiram, A. Phloroglucinol–2,6-Diaminoanthraquinone as a Durable Redox Mediator for Enhancing Conversion Reaction Kinetics in Lithium-Sulfur Batteries. Adv. Funct. Mater. 2024, 2405814-2405822.

[2] Zheng, Q.; Fan, X.; Liu, G.; Hou, Q.; Fan, J.; Zheng, M.; Dong, Q. Enhancing sulfur cathode process via a functionalized complex molecule. Nano Res. 2022, 16 (6), 8385-8393.

[3] Q. Hou, K. Wang, W. Zheng, X. Li, M. Yu, H. Jiang, Y. Dai, F. Chu, X, Jiang, D. Zhu, G. He, Eliminating bandgap between Cu-$CeO_{2-x}$ heterointerface enabling fast electron transfer and redox reaction in Li-S batteries. Energy Storage Mater. 63 (2023) 102983.

[4] L. Wang, X. Yin, B. Li, G. Zheng, Mixed Ionically/Electronically Conductive Double-Phase Interface Enhanced Solid-State Charge Transfer for a High-Performance All-Solid-State Li–S Battery. Nano Lett. 22 (2021) 433-440.

[5] Li, J.; Wang, Z.; Shi, K.; Wu, Y.; Huang, W.; Min, Y.; Liu, Q.; Liang, Z. Nanoreactors Encapsulating Built-in Electric Field as a "Bridge" for Li–S Batteries: Directional Migration and Rapid Conversion of Polysulfides. Adv. Energy Mater. 2023, 14 (9), 2303546-2303558.

[6] Y. Li, J. Wu, B. Zhang, W. Wang, G. Zhang, Z. Seh, N. Zhang, J. Sun, L. Huang, J. Jiang, J. Zhou, Y. Sun, Fast conversion and controlled deposition of lithium (poly)sulfides in lithium-sulfur batteries using high-loading cobalt single atoms. Energy Storage Mater. 30 (2020) 250-259.

[7] C. Qi, Z. Li, C. Sun, C. Chen, J. Jin, Z. Wen, Cobalt Phosphide Nanoflake-Induced Flower-like Sulfur for High Redox Kinetics and Fast Ion Transfer in Lithium-Sulfur Batteries. ACS Appl Mater Inter. 12 (2020) 49626-49635.

[8] Jiao, L.; Jiang, H.; Lei, Y.; Wu, S.; Gao, Q.; Bu, S.; Kong, X.; Yang, S.; Shu, D.; Li, C.; Li, H.; Cheng, B.; Lee, C.; Zhang, W. "Dual Mediator System" Enables Efficient and Persistent Regulation toward Sulfur Redox Conversion in Lithium–Sulfur Batteries. ACS Nano, 2022, 16 (9), 14262-14273.

[9] Zhou, Y.; Zhang, Y.; Li, X. Upcycling of paper waste for high-performance lithium-sulfur batteries. Mater. 2021, 19, 1-37.

[10] C. Zha, X. Zhu, J. Deng, Y. Zhou, Y. Li, J. Chen, P. Ding, Y. Hu, Y. Li, H. Chen, Facet-tailoring five-coordinated Ti sites and structure-optimizing electron transfer in a bifunctional cathode with titanium nitride nanowire array to boost the performance of $Li_2S_6$-based lithium–sulfur batteries. Energy Storage Mater. 26 (2020) 40-45.

[11] Z. Li, J. Zhang, B. Guan, D. Wang, L.-M. Liu, X. Lou, A sulfur host based on titanium monoxide@carbon hollow spheres for advanced lithium–sulfur batteries. Nat. Commun. 7 (2016) 13065-13076.

[12] C. Zha, X. Gu, D. Wu, H. Chen, Interfacial active fluorine site-induced electron transfer on $TiO_2$ (001) facets to enhance polysulfide redox reactions for better liquid $Li_2S_6$-Based lithium–sulfur batteries. J. Mater. Chem. A. 7 (2019) 6431-6438.

[13] Sun, W.; Xu, Y.; Chen, X.; Xu, Y.; Wu, F.; Wang, Y. Reduced graphene oxide modified with naphthoquinone for effective immobilization of polysulfides in high-performance Li-S batteries. Chem. Eng. J. 2020, 383, 1-53.

[14] L.-P. Hou, H. Yuan, C.-Z. Zhao, L. Xu, G.-L. Zhu, H.-X. Nan, X.-B. Liu, Q.-B. Liu, C.-X. He, J.-Q. Huang, Q. Zhang, Improved interfacial electronic contacts powering high sulfur utilization in all-solid-state lithium–sulfur batteries. Energy Storage Mater. 25 (2020) 436-442.

[15] Y. Xu, W. Yuan, C. Geng, Z. Hu, Q. Li, Y. Zhao, X. Zhang, Z. Zhou, C. Yang, Q.-H. Yang, High-Entropy Catalysis Accelerating Stepwise Sulfur Redox Reactions for Lithium–Sulfur Batteries. Adv. Sci. 11 2024 2402497-2402506

[16] Y. Ding, Z. Shi, Y. Sun, J. Wu, X. Pan, J. Sun, Steering Bidirectional Sulfur Redox via Geometric/Electronic Mediator Comodulation for Li–S Batteries. ACS Nano, 17 (2023) 6002-6010.